universität wien

MASTERARBEIT / MASTER'S THESIS

Titel der Masterarbeit / Title of the Master's Thesis

„Trapping Potentials and Numerics for Gross-Pitaevskii type Equations“

verfasst von / submitted by

Charlotte Anna Bode

angestrebter akademischer Grad / in partial fulfilment of the requirements for the degree of

Master of Science (MSc)

Wien, 2019 / Vienna, 2019

Studienkennzahl lt. Studienblatt / degree programme code as it appears on the student record sheet:	UA 066 910
Studienrichtung lt. Studienblatt / degree programme as it appears on the student record sheet:	Masterstudium Computational Science
Betreut von / Supervisor:	Univ.-Prof. Dr. Norbert Mauser

Abstract

The nonlinear Schrödinger equation (NLSE) is a partial differential equation with many applications in quantum physics, nonlinear optics, etc. In this thesis, selected numerical methods to deal with dynamical as well as ground state computations of the nonlinear Schrödinger equation are presented with a special focus on the cubic NLSE, also known as the Gross-Pitaevskii equation (GPE), a standard model for Bose-Einstein Condensates (BECs). For such GPEs, we investigate numerical performance and accuracy of a Time Splitting Spectral Method (TSSM) and a Backward Euler Finite Difference (BEFD) Method.

We introduce the physics including the scaling of BECs and present some dynamical properties of GPEs. Then, the mathematical theory of the nonlinear eigenvalue problem, which models stationary states of BECs, is briefly discussed. Furthermore, we examine numerical aspects of finding ground state solutions. In particular, a normalized gradient flow method is provided to obtain ground state solutions by propagating an imaginary time. Once the theory of numerical methods is investigated, an adaptive temporal step size adjustment is established to guarantee a fast and accurate convergence of ground state solutions.

A special focus lies on the investigation of different confining potentials and their influence on numerical accuracy. Due to discontinuities arising from box potentials with sharp edges a special numerical treatment is required. A detailed analysis of box potentials and their defining parameters with respect to the required spatial resolution is proposed. We examine the influence of the layer size, the height and the nonlinearity constant on time propagation as well as ground state solutions.

Finally, we conclude by presenting numerical results for both dynamics as well as ground state computations in two and three dimensions.

Deutsche Zusammenfassung

Diese Arbeit beschäftigt sich mit numerischen Methoden für das Lösen der Gross-Pitaevskii Gleichung (GPG). Die GPG beschreibt die zeitliche Entwicklung von Bose-Einstein Kondensaten.

Im Rahmen dessen werden zwei numerische Methoden eingeführt, die *Time Splitting Spectral* Methode (TSSM) und die *Backward Euler Finite Difference* (BEFD) Methode, mit Hilfe derer sowohl Grundzustands- als auch Zeitevolutionsrechnungen durchgeführt werden. Ein besonderes Augenmerk liegt auf der numerischen Analyse eines Box-Potentials. Insbesondere im Hinblick auf die Wahl der räumlichen Auflösung werden verschiedene Parameter eines Box-Potentials untersucht.

Außerdem wird eine Methode entwickelt, um die Zeitschritte während der Grundzustandsrechnung zu verkleinern: mit dem Ziel, mit wenig Iterationen besonders genaue Grundzustände zu erreichen. Die Grundidee basiert auf der Halbierung des Zeitschritts, sobald sich die Lösung über einen gewissen Zeitraum nicht mehr signifikant ändert.

Am Schluss werden Rechenergebnisse präsentiert, die durch eine MATLAB Implementierung erzeugt und auf einer GPU parallelisiert werden. Dabei werden die numerischen Methoden TSSM und BEFD in einer Dimension auf ihre Ordnungen in Zeit und Raum analysiert. Schließlich werden Anwendungsergebnisse in zwei und drei Dimensionen präsentiert.

Acknowledgements

First of all I want to thank Prof. Dr. Norbert J. Mauser for excellent lectures in Numerical PDE topics and for giving me the opportunity to write this thesis. Everytime we met and talked about this topic, I was inspired by his insights and intuition in physics.

Also I want to thank all the members of the WPI c/o Fakultät Mathematik. In particular, I want to thank Jan-Frederik Mennemann and Hans-Peter Stimming who provided some key ideas and were very helpful with many remarks and corrections concerning numerical algorithms and implementation.

Furthermore, I gratefully acknowledge the financial support by the Austrian Science Foundation (FWF) via the grant No F65 (¨SFB Complexity in PDEs¨) .

I also wish to thank my fellow students Jakob Weber, Konrad von Kirchbach, Nadja Singer and Wolfgang Ost for motivating and funny discussions during umpteen lunches throughout the entire master.

Arndt, Anja, Archie and Max – thank you for your support.

Contents

List of Symbols

$\mathbb{R}$	Set of Real Numbers
$d = 1, 2, 3$	Spatial Dimension
$\mathbf{x}$	Position Variable
t	Time Variable
i	Imaginary Unit
$\hbar$	Reduced Planck Constant
m	Atomic Mass
N	Number of Atoms in Condensate
ψ	Time-Dependent Wavefunction
ϕ	Time-Independent Wavefunction
ψ_0	Initial Data
V	External Potential
E	Total Energy
μ	Chemical Potential
ϕ_g	Ground State Wavefunction
λ	Nonlinearity Constant
$\omega_x, \omega_y, \omega_z$	Trapping Frequencies in x-, y-, z- Direction
∇	Gradient Operator
Δ	Laplacian Operator
$\frac{\partial}{\partial t}$	Partial Derivative w.r.t. time
Δx	Spatial Stepsize
Δt	Temporal Stepsize
$\|\cdot\|_{\mathbb{L}^2}$	$\mathbb{L}^2$ Function Norm
n	Number of Time Steps
M	Number of Spatial Grid Points
x_j	j-th Spatial Grid Point
t_n	Discretized Time Level $n\Delta t$
ϕ_j^n	Solution at Grid Point x_j and Time t_n
$D_2^{1/2}$	Second Order Central Finite Difference Approximation of 1st/2nd derivative
$D_4^{1/2}$	Fourth Order Central Finite Difference Approximation of 1st/2nd derivative

Part I

Introduction

Chapter 1

Gross-Pitaevskii Equation

1.1 Motivation

Nonlinear Schrödinger type equations (NLSEs) are a large class of dispersive partial differential equations (PDEs), which appear in many applications in quantum physics, nonlinear optics, etc. A particular interest on NLSE lies in quantum physics as a model for Bose-Einstein condensates (BECs).

The Bose-Einstein condensate is a dilute gas of bosons, in which particles have the property to occupy the same one-particle quantum state which occurs at zero or sufficiently low temperature (then the majority of particles are in the same quantum state).

The phenomenon at which quantum microscopic matter becomes mesoscopic was first predicted in 1924 by Satyendra Bose and Albert Einstein in [Bos24]. An experimental realization was later produced by Eric A. Cornell, Carl E. Wieman and a team of physicists at the Joint Institute for Laboratory Astrophysics (JILA) in 1995 (see [AEM+95, CW98]). The condensation was initially achieved with rubidium atoms at a temperature of minus 273.15° Celsius in a laboratory at JILA. Similarly, for a gas of sodium atoms condensation was realized by Wolfgang Ketterle at MIT. In 2001, Cornell, Wieman and Ketterle received the Nobel Price in Physics for their work.

BECs are mathematically most simply modelled by the Gross-Pitaevskii equation (GPE) which is a NLSE with local cubic nonlinearity. [BC12, HLSPSY06, JL01, PS04] derive the GPE by a weak coupling/mean field limit from the linear N-body Schrödinger equation.

The GPE in $d > 0$ dimensions for a domain $\Omega \subseteq \mathbb{R}^d$ has the following form

$$i\hbar\frac{\partial}{\partial t}\psi(x,t) = -\frac{\hbar^2}{2m}\Delta\psi(\mathbf{x},t) + V(\mathbf{x})\psi(\mathbf{x},t) + Ng|\psi(\mathbf{x},t)|^2\psi(\mathbf{x},t) \quad \mathbf{x}\in\Omega,\ t\in\mathbb{R} \tag{1.1.1}$$

$$\psi(\mathbf{x},0) = \psi_0(\mathbf{x}) \qquad \mathbf{x}\in\Omega \tag{1.1.2}$$

where $\Delta = div(grad(\cdot))$ denotes the Laplace operator, $\mathbf{x}$ the position vector, m the atomic mass, $\hbar$ the Planck constant, N the number of atoms in the condensate and the constant $g = \frac{4\pi\hbar^2 a_s}{m}$. Here $a_s = 5.1 \times 10^{-9} m$ is the corresponding scattering length of bosons. In the case of a harmonic oscillator as trap potential $V(\mathbf{x}) = \frac{m}{2}\left(\omega_x^2 x^2 + \omega_y^2 y^2 + \omega_z^2 z^2\right)$ with $\omega_x, \omega_y, \omega_z$ trap frequencies in x, y and z-direction.

The corresponding energy expression has the form

$$E_g(\psi) := \int_\Omega \left[\frac{\hbar^2}{2m}|\nabla\psi(\mathbf{x},t)|^2 + V(\mathbf{x})|\psi(\mathbf{x},t)|^2 + \frac{Ng}{2}|\psi(\mathbf{x},t)|^4\right] d\mathbf{x}$$

(see [BC12]).

Following [BC12] we want to nondimensionalize equation (1.1.1)–(1.1.2). We introduce

$$\tilde{t} = \frac{t}{t_s}, \qquad \tilde{\mathbf{x}} = \frac{\mathbf{x}}{x_s},$$
$$\tilde{\psi}(\tilde{\mathbf{x}}, \tilde{t}) = x_s^{\frac{3}{2}}\psi(\mathbf{x}, t)$$

where t_s, x_s are the scaling parameters of dimensionless units chosen as

$$t_s = \frac{1}{\omega_x} \qquad x_s = \sqrt{\frac{\hbar}{m\omega_x}}$$

x_s denotes the length of the harmonic ground state in x-direction.

Inserting the new variables into (1.1.1)-(1.1.2), multiplying by $\frac{1}{m\omega_x^2 x_s^{1/2}}$ and finally removing all $\tilde{}$ the following dimensionless GPE is obtained

$$i\frac{\partial}{\partial t}\psi(x,t) = -\frac{1}{2}\Delta\psi(\mathbf{x},t) + V(\mathbf{x})\psi(\mathbf{x},t) + \lambda|\psi(\mathbf{x},t)|^2\psi(\mathbf{x},t) \quad \mathbf{x}\in\Omega,\ t\in\mathbb{R} \quad (1.1.3)$$
$$\psi(\mathbf{x},0) = \psi_0(\mathbf{x}) \quad \mathbf{x}\in\Omega \quad (1.1.4)$$

where the dimensionless interaction parameter λ is given by $\lambda = \frac{4\pi N a_s}{x_s}$, $V(\mathbf{x}) = \frac{1}{2}\left(x^2 + \gamma_y^2 y^2 + \gamma_z^2 z^2\right)$, $\gamma_y = \frac{\omega_y}{\omega_x}$ and $\gamma_z = \frac{\omega_z}{\omega_x}$ and
See [BC12] for a complete description of the scaling and the choice of scaling parameters corresponding to different external trapping potentials.

The parameter λ describes the strength of interactions and is positive for repulsive/defocusing interaction and negative for attractive/focusing interaction.

In (1.1.3) $V(\mathbf{x})$ is a real-valued trapping potential, which can assume different forms according to the application.

The aim of this thesis is to investigate several numerical methods to deal with ground state computations as well as dynamics of the GPE. In particular, a numerical treatment of a box potential as trapping potential for the condensate is intensively analysed. While harmonic or double well potentials are numerically favourable because of their smoothness, numerics for box potential has to

deal with sharp edges. The basic question in this context is whether numerical methods, which are widely used for smooth potentials, can be applied for box potentials.

Ground states can be numerically achieved by imaginary time propagation (see [LTE07]) where applying $t \to -it$ instead of real time steps yields ground state solutions. Spectral methods with their highly efficient Fast Fourier transforms in combination with an operator splitting approach are amongst the most popular tools for solving the imaginary time propagation problem. However, the choice of the time step is crucial to produce numerically accurate solutions. Another focus of this thesis is therefore to investigate an approach in which the temporal step size is dynamically adapted during the computation.

1.2 Dynamical Properties

We now list some dynamical properties, which are used to evaluate the numerical methods in part III. Therefore, the following chapter briefly recalls properties of (1.1.3)-(1.1.4).

Among these properties there are two important invariants:
mass conservation:

$$N(\psi) = \|\psi(\cdot, t)\|^2 = \int_\Omega |\psi(\mathbf{x}, t)|^2 \, d\mathbf{x} = 1, \quad t \geqslant 0 \tag{1.2.1}$$

energy conservation:

$$E(\psi(\cdot, t)) = \int_\Omega \left[\frac{1}{2} |\Delta\psi(\mathbf{x}, t)|^2 + V(\mathbf{x}) |\psi(\mathbf{x}, t)|^2 + \frac{\lambda}{2} |\psi(\mathbf{x}, t)|^4 \right] d\mathbf{x} \tag{1.2.2}$$

Note, a normalization to the number of atoms N in the condensate is achieved by rescaling (1.1.1) by $\psi \to \frac{1}{\sqrt{N}}\psi$.

Moreover, we have the following dynamical properties (see [ABB13]), which will be used to evaluate numerical schemes afterwards:

- *time reversible/symmetric*: unchanged under change of variable $t \to -t$ and complex conjugation of the equation
- *time transverse/gauge invariant*: if $V \to V + \alpha$ for $\alpha \in \mathbb{R}$ then $\psi \to \psi e^{-i\alpha t}$
- *admits plane wave solution* $A e^{i(\mathbf{k}\cdot\mathbf{x} - \omega t)}$ with time frequency ω, amplitude A and spatial wave number $\mathbf{k}$ satisfying dispersion relation

$$\omega = \frac{|\mathbf{k}|^2}{2} + \lambda |A|^2$$

Note, that these concepts are valid for all dimensions $d \geqslant 1$, however in this thesis we restrict the numerics of the GPE (1.1.3)-(1.1.4) to $d = 1, 2, 3$.

Chapter 2

Trapping Potentials

In this chapter we briefly present some particular trapping potentials for the GPE (1.1.3) - (1.1.4), with a special focus on box potentials.
A main part of this thesis is the numerical investigation of box potentials with respect to required resolutions. Due to a particular smoothed potential obtained by using the tanh-function, we examine three parameters defining the box potential as well as the solution of the GPE.

This chapter will give a brief introduction of the used potentials. Later a detailed numerical analysis is given in chapter 10.

As we consider the equation in dimensionless form, the following confining potentials are also nondimensionalized.

- Harmonic Oscillator for trap frequencies $\omega_x, \omega_y, \omega_z$
  - 1D: $V(x) = \frac{1}{2}\omega_x x^2$
  - 2D: $V(x,y) = \frac{1}{2}(x^2 + \gamma_y^2 y^2)$ with $\gamma_y = \frac{\omega_y}{\omega_x}$
  - 3D: $V(x,y,z) = \frac{1}{2}(x^2 + \gamma_y^2 y^2 + \gamma_z^2 z^2)$ with $\gamma_y = \frac{\omega_y}{\omega_x}$ and $\gamma_z = \frac{\omega_z}{\omega_x}$

  For the choice of nondimensionalization parameters of chapter 1 according to the different external potentials see [BC12].

- Box Potential
  - Box with sharp edges

$$V(\mathbf{x}) = \begin{cases} 0, & |\mathbf{x}| \leqslant \frac{1}{2}w \\ h, & otherwise \end{cases}$$

    where h denotes the height of the box potential and w the width. From the numerical point of view, sharp edges are causing issues concerning numerical accuracy. Therefore, we introduce a particular smoothing which uses the tanh-function to define the edges.

– Box potential with smoothed edges by using tanh

$$V = h * \frac{\tanh(\frac{1}{d} * (|x| - \frac{w}{2.0})) + 1.0)}{2} \tag{2.0.1}$$

with h height and w width of the box (see figure 2.1a).
$1/d$ denotes the size of the "layer" of tanh, i.e. the x values for which the tanh function values are not constant (see figure 2.1b).

Note, that this definition can be generalized for more than one dimension. Then, V is distinctly defined in each direction, which enables the combination of various kinds of potentials (e.g. in 3d: harmonic potential in x direction, box potential in y direction, double well potential in z direction).

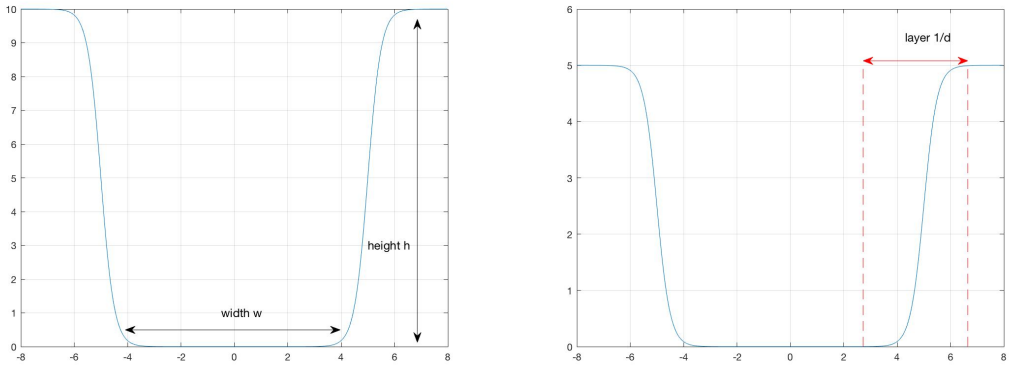

(a) (b)

Figure 2.1: *Defining Box Parameters*

In chapter 10 we analyse the numerical performance and accuracy of box potentials with respect to three parameters:

– Layer size $1/d$ (see figure 2.1b)
– Height h (see figure 2.1a)
– Nonlinearity constant g

We will investigate whether a particular numerical treatment is required, as these parameters vary.

Part II

Computing Ground States

Chapter 3

Stationary States

Computing a stationary state consists of finding a solution

$$\psi(\mathbf{x}, t) = e^{-i\mu t}\phi(\mathbf{x}) \tag{3.0.1}$$

where μ denotes the chemical potential of the BEC and ϕ a time-independent function. Inserting (3.0.1) into (1.1.3), we obtain the nonlinear elliptic equations for $(\mu, \phi(\mathbf{x}))$

$$\mu\phi(\mathbf{x}) = -\frac{1}{2}\Delta\phi(\mathbf{x}, t) + V(x)\phi(\mathbf{x}, t) + \lambda|\phi(\mathbf{x}, t)|^2\phi(\mathbf{x}, t) \tag{3.0.2}$$

with the normalization constraint

$$\|\phi\|_{\mathbb{L}^2} = \int_\Omega |\phi(\mathbf{x}, t)|^2 d\mathbf{x} = 1 \tag{3.0.3}$$

The eigenvalue of the nonlinear eigenvalue problem is given by

$$\begin{aligned}\mu = \mu_\lambda &= \int_\Omega \frac{1}{2}|\nabla\phi(\mathbf{x}, t)|^2 + V(\mathbf{x})|\phi(\mathbf{x}, t)|^2 + \lambda|\phi(\mathbf{x}, t)|d\mathbf{x} \\ &= E_\lambda(\phi) + \int_\Omega \frac{\lambda}{2}|\phi(\mathbf{x})|^2 d\mathbf{x}\end{aligned}$$

Then, the ground state of a non-rotating BEC can be found by minimizing the energy functional $E_\lambda(\phi)$ under the constraint (3.0.3), i.e.
Find $\phi_g \in S := \{\phi| \ \|\phi\|^2 = 1, E_\lambda(\phi) < \infty\}$ such that

$$E_g := E_\lambda(\phi_g) = min_{\phi\in S} E_\lambda(\phi)$$

For existence and uniqueness of these ground states see [BC12]. They proved a justification for choosing nonnegative ground states, therefore we restrict on real valued wave functions.

For trapping potentials the ground state solution decays exponentially fast as $|\mathbf{x}| \to \infty$ (see chapter 2.1.2 in [BC12]. Therefore, it is natural to truncate (1.1.3) – (1.1.4) to a bounded domain U.

Chapter 4

Normalized Gradient Flow

4.1 Imaginary Time Propagation – Gradient Flow with Normalized Discretization

There are several numerical methods for computing the ground state solution of BECs. [BT09] presents approximate ground state solutions in two extreme regimes by directly minimizing the energy functional. Moreover, [AD14] give an approach based on Krylov subspace solvers with a Laplace and Thomas-Fermi preconditioner.
A very popular approach in the physics literature is the *imaginary time propagation* method, which [BD04] introduced as *Gradient Flow with Discrete Normalization* (GFDN).
By inserting $t \to -it$ into (1.1.3)-(1.1.4) the following GFDN can be obtained:

$$\partial_t \phi = \frac{1}{2}\Delta\phi - V(\mathbf{x})\phi - \lambda|\phi|^2\phi \qquad x \in U, t_n < t < t_{n+1}, n \geqslant 0 \qquad (4.1.1)$$

$$\phi(\mathbf{x}, t) \hat{=} \phi(\mathbf{x}, t_{n+1}^+) = \frac{\phi(\mathbf{x}, t_{n+1}^-)}{\|\phi(\cdot, t_{n+1}^-)\|} \qquad x \in U, n \geqslant 0 \qquad (4.1.2)$$

$$\phi(\mathbf{x}, t) = 0, \quad x \in \partial U, \qquad \phi(\mathbf{x}, 0) = \phi_0(\mathbf{x}), \ x \in U \qquad (4.1.3)$$

where $\phi(\mathbf{x}, t_n^{\pm}) = \lim_{t \to t_n^{\pm}} \phi(\mathbf{x}, t)$, $\|\cdot\| = \|\cdot\|_{L^2(U)}$ and $\|\phi_0\| = 1$.

Consider the following series of discretized time steps, i.e $t_0 < t_1 < ... < t_N$ with $t_{n+1} - t_n = \Delta t_n =: k_n$ for $j = 0, .., N-1$ for $N \in \mathbb{N}$ the number of time steps. The wave function ϕ is normalized by projecting the solution back on the unit sphere after each time step.

Since the RHS of (4.1.1) is equal to $-\frac{1}{2}\frac{\delta E_\lambda(\phi)}{\delta\phi}$, (4.1.1) is comparable with a steepest descent approach applied to the energy functional $E_\lambda(\phi)$.

[BD04] proved that for $V(\mathbf{x}) \geqslant 0$ for all $x \in U$, $\|\phi_0\| = 1$ and $\lambda = 0$ GFDN is

energy diminishing for any time step $k := max_{n<N} k_n$ and initial data ϕ_0, i.e.

$$E_0(\phi(\cdot, t_{n+1})) \leqslant E_0(\phi(\cdot, t_n)) \leqslant ... \leqslant E_0(\phi(\cdot, 0)) = E_0(\phi_0), n = 0, 1, 2, ...$$

This gives a justification for computing ground state solutions of BECs by GFDN in the linear regime ($\lambda = 0$).
However, for $\lambda \geqslant 0$ a similar statement is no longer valid, since the diminishing property is not preserved over the normalization constraint (4.1.2). In particular, for $\lambda \geqslant 0$ only

$$E(\phi(\cdot, t)) \leqslant E(\phi(\cdot, t')) \qquad t_n \leqslant t < t' \leqslant t_{n+1}$$

can be shown. Note that ground state solutions can only be computed for $\lambda \geqslant 0$. Therefore the case of $\lambda < 0$ is note included here.

4.2 Continuous Normalized Gradient Flow

[BD04] introduces another method including continuous coefficients. In particular, including the constraint (4.1.2) into the Gradient Flow (4.1.1) yields a first order splitting with discontinuous coefficients depending on the time step k_n

$$\partial_t \phi = \frac{1}{2}\Delta\phi - V(\mathbf{x})\phi - \lambda|\phi|^2\phi + \mu_\phi(t, k)\phi \qquad x \in U, t_n < t < t_{n+1}, n \geqslant 0$$
$$\phi(\mathbf{x}, t) = 0, \quad x \in \Gamma, \qquad \phi(\mathbf{x}, 0) = \phi_0(\mathbf{x}), \ x \in U$$

where

$$\mu_\phi(t, k) \equiv \mu_\phi(t_{n+1}, \Delta t_n) = -\frac{1}{2k_n} \ln \|\phi(\cdot, t_{n+1}^-)\|^2 \qquad t_n \leqslant t \leqslant t_{n+1} \tag{4.2.1}$$

Letting $k_n \to 0$ we obtain

$$\mu_\phi(t) = \frac{1}{\|\phi(\cdot, t)\|^2} \int_\Omega \left[\frac{1}{2}|\nabla\phi(\mathbf{x}, t)|^2 + V(x)\phi^2(\mathbf{x}, t) + \lambda\phi(\mathbf{x}, t)^4\right] d\mathbf{x} \tag{4.2.2}$$

That's how the *Continuous Normalized Gradient Flow* (CNGF) is derived:

$$\partial_t \phi = \frac{1}{2}\Delta\phi - V(\mathbf{x})\phi - \lambda|\phi|^2\phi + \mu_\phi(t)\phi \qquad x \in U, t \geqslant 0 \tag{4.2.3}$$
$$\phi(\mathbf{x}, t) = 0, \quad x \in \Gamma, \qquad \phi(\mathbf{x}, 0) = \phi_0(\mathbf{x}), \ x \in U \tag{4.2.4}$$

For CNGF [BD04] proves the energy diminishing property also for $\lambda \geqslant 0$

Part III

Efficient and Accurate Numerical Methods

Chapter 5

Discretization

The following chapter introduces some efficient and accurate methods for computing the time evolution as well as computing ground state solutions of Bose-Einstein Condensates.

In part IV the methods are compared based on numerical results with a focus on an accurate performance for box potentials.

For simplicity the notation is introduced in one dimension, i.e. $d = 1$. A generalization for $d > 1$ can be derived analogously. Let $I_j := \{j \mid 0, ..., M-1\}$ be the spatial discretization index set.
For a bounded domain $U = [a, b]$ and a nonnegative number $M > 0$ let $\{x_j\}_{j \in I_j}$ be the grid points in an equidistant grid:

$$\begin{aligned} &x_0 = a \\ &x_{M-1} = b \\ &h := \Delta x = x_{j+1} - x_j \qquad\qquad j \in I_j \end{aligned}$$

Note that depending on the used numerical scheme the last grid point might be identified with $x_{M-1} = b - \Delta x$ (for the case of Time Splitting Spectral method). Let $\{t_n\}_{n=0,1,...}$ denote the discretization in time, where

$$k_n := \Delta t_n = t_{n+1} - t_n$$

is the temporal step size, which does not have to be equidistant. Note that both sequences $\{x_j\}_{j \in I_j}$ as well as $\{t_n\}_{n=0,1,...}$ are chosen such that they are monotonously increasing.

Then ϕ^n is the solution vector at time $t = t^n$ consisting of the components ϕ_j^n, which represents the numerical approximation of ϕ at the grid points (x_j, t_n).

Note that the choice of boundary conditions is related to the different numerical methods. A brief remark is given in each chapter respectively.

For the solution ϕ^n define the discrete l^p and l^∞ norm as

$$\|\phi^n\|_p^p := h \sum_{j \in I_j} |\phi_j^n|^p \qquad \|\phi^n\|_\infty := \sup_{j \in I_j} |\phi_j^n|$$

Moreover define the following centered finite difference approximations for spatial discretization:

$$\begin{aligned}
D_2^1 &:= -\frac{1}{2h}\left(\phi_{j-1}^n - \phi_{j+1}^n\right) \\
D_4^1 &:= \frac{1}{h}\left(\frac{1}{12}\phi_{j-2}^n - \frac{2}{3}\phi_{j-1}^n + \frac{2}{3}\phi_{j+1}^n - \frac{1}{12}\phi_{j+2}^n\right) \\
D_2^2 &:= \frac{1}{h^2}\left(\phi_{j-1}^n - 2\phi_j^n + \phi_{j+1}^n\right) \\
D_4^2 &:= \frac{1}{h^2}\left(-\frac{1}{12}\phi_{j-2}^n + \frac{4}{3}\phi_{j-1}^n - \frac{5}{2}\phi_j^n + \frac{4}{3}\phi_{j+1}^n - \frac{1}{12}\phi_{j+2}^n\right)
\end{aligned}$$

The lower index $\{2, 4\}$ represents a second or fourth order approximation, whereas the upper index specifies the order of the derivative to approximate.

The following chapters introduce two numerical methods, which are widely used for the GPE.

Chapter 6

Time Splitting Spectral Method

6.1 Split Step Methods

The main idea of *Time Split step methods* is to split up an initial value problem with two operators A, B

$$\partial_t u = Au + Bu \quad t \geqslant 0 \tag{6.1.1}$$

with $u = u(\mathbf{x}, t) \in \mathbb{R}^d \times \mathbb{R}$ and solve them independently per time step.
Considering exponential operator splitting (see [DT19]) for the time integration of (6.1.1) yields an approximation of the exact solution:

$$u^n = \prod_{j=1}^{s} e^{a_j kA} e^{b_j kB} u^{n-1} \quad n > 1,$$

for given initial data u_0, appropriate coefficients a_j, b_j and a time step k.
The *Lie-Trotter formula* (see [Tro59]) is an example for a *first order splitting* with $s = 1, a_1 = 1, b_1 = 1$
The *Strang formula* (see [Str68]) which is derived by symmetrizing Lie Trotters formula is a *second order splitting* with coefficients
$s = 2, a_1 = \frac{1}{2}, b_1 = 1, a_2 = \frac{1}{2}, b_2 = 0$
For a convergence analysis see [NT09, Thao8, Tha12].

Applied to the Gross-Pitaevskii equation, (1.1.3)-(1.1.4) is splitted into two operators, the Laplacian

$$A = -\frac{1}{2}\Delta$$

for the free evolution and the potential operator

$$B = V + \lambda |u|^2$$

for the nonlinear part. Therefore, the cubic NLSE converts to

$$i\partial_t u = (A + B)u$$

$$u(\cdot, 0) = u_0(\cdot)$$

Beginning with the flow e^{kB} for the potential part of the equation

$$i\partial_t w = V_w + c|w|^2 w \qquad \mathbf{x} \in \Omega, t > 0 \tag{6.1.2}$$

$$w(\mathbf{x}, 0) = w_0(\mathbf{x}) \qquad \mathbf{x} \in \Omega \tag{6.1.3}$$

we observe that multiplying the equation by $\bar{w}$ yields

$$\frac{i}{2}\partial_t(|w|^2) = V_{ext}|w|^2 + g(|w|^2)|w|^2$$

Taking the imaginary part, we are left over with $\partial_t(|w|^2) = 0$, which directly implies that

$$|w(\mathbf{x}, t)|^2 = const. = |w_0(\mathbf{x})|^2$$

Note, that the external potential is chosen as a positive real-valued function. Therefore, (6.1.2) – (6.1.3) can be integrated exactly and we obtain

$$w(\mathbf{x}, t) = e^{-\frac{i}{2}t(V+g(|w|^2))}w(\mathbf{x}, t)$$

The flow e^{kA} of the free part of the equation

$$i\partial_t v = -\frac{1}{2}\Delta v \qquad \mathbf{x} \in \Omega, t > 0 \tag{6.1.4}$$

$$v(\mathbf{x}, 0) = v_0(\mathbf{x}) \qquad \mathbf{x} \in \Omega \tag{6.1.5}$$

can be solved by any numerical method.

6.2 Time Splitting Spectral Method

Spectral methods yield highly accurate results for smooth numerical problems such as ground state computations with smooth confining potentials and periodic boundary conditions. Due to the efficient implementation of *Fast Fourier Transform*, spectral methods are also very favourable in terms of computational runtime. We use spectral methods for solving the flow e^{kA} ((6.1.4) – (6.1.5)) and combine both flows by Strang's formula. This yields the following discretization scheme of the gradient flow (4.1.1) – (4.1.3):

$$u_j^\star = e^{-\frac{i}{2}k(V_{ext}(x_j)+g(|u_j^n|^2))}u_j^n \qquad j = 0, 1, .., M-1 \tag{6.2.1}$$

$$u_j^{\star\star} = \frac{1}{M}\sum_{l=-\frac{M}{2}}^{\frac{M}{2}-1} e^{-\frac{i}{2}k\mu_l^2}(\hat{u^\star})_l e^{i\mu_l(x_j-a)} \qquad j = 0, 1, ..., M-1 \tag{6.2.2}$$

$$u_j^{n+1} = e^{-\frac{i}{2}k(V_{ext}(x_j)+g(|u_j^{\star\star}|^2))}u_j^{\star\star} \qquad j = 0, 1, .., M-1 \tag{6.2.3}$$

where $(\hat{u^\star})_l$ are the Fourier coefficients of $(u^\star)$ defined as

$$(\hat{u^\star})_l := \sum_{j \in I_j} u_j^\star e^{-i\mu_l(x_j - a)}, \quad \mu_l = \frac{2\pi l}{b-a}, \quad l = -\frac{M}{2}, ..., \frac{M}{2} - 1$$

Another splitting method is proposed by [BM02]:

$$e^{b_1 kB} e^{a_1 kA} ... e^{b_s kB} e^{a_s kA} e^{b_{s+1} kB} \tag{6.2.4}$$

with $s = 6$ and $a_{s+1-i} = a_i$ and $b_{s+2-i} = b_i$ for the coefficients:

j	a_j	j	b_j
1, 6	0.245298957184271	1,7	0.0829844064174052
2, 5	0.604872665711080	2,6	0.396309801498368
3, 4	$\frac{1}{2} - (a_1 + a_2)$	3,5	- 0.0390563049223486
		4	$1 - 2(b_1 + b_2 + b_3)$

Table 6.1: 4th order splitting method

It is a 4th order splitting method and therefore decreases the temporal error, see [TCN09] for a detailed convergence analysis.

6.3 Computational Remarks

The presented TSSM is unconditionally stable and satisfies a first, second or fourth order accuracy in time (Lie-Trotter, Strang or (6.2.4) splitting). Moreover spectral methods yield a spectral order accuracy in space. For both see [Tha12]. In chapter 9 we compare the numerical performance and accuracy of the three splitting schemes.
The memory effort for d dimensions is $\mathcal{O}(M^d)$ and runtime per time step scales in $\mathcal{O}(M \log M)$ because of the highly efficient *Fast Fourier Transform* algorithm.

In terms of time propagation, TSSM appears to be a good choice. The scheme (6.2.1)-(6.2.3) preserves almost all dynamical properties of the solution of the GPE explained in chapter 1.2. In particular, it is time reversible, symmetric and time transverse. It conserves mass and the dispersion relation stays valid, however performing dynamics of GPE with TSSM does not conserve energy.

To apply Fourier Spectral methods we impose periodic boundary conditions on the bounded domain U.

Chapter 7

Backward Euler Finite Difference

In this section a *Backward Euler Finite Difference* (BEFD) scheme is constructed by discretizing (4.1.1)- (4.1.3) by a finite difference scheme.
In particular, we use the *Backward Euler* in time and a centered finite difference approximation in space. Therefore, we obtain for the normalized gradient flow:

$$\begin{aligned}
&\frac{\phi_j^\star - \phi_j^n}{k} = \frac{1}{2}\left(D_{2,4}^2\phi^\star\right) - V(x_j)\phi_j^\star - c(\phi_j^n)^2\phi_j^\star, && j = 1, ..., M-1\\
&\phi_0^\star = \phi_M^\star = 0, \quad \phi_j^0 = \phi_0(x_j), && j = 0, 1, ..., M\\
&\phi_j^{n+1} = \frac{\phi_j^\star}{\|\phi^\star\|}, && j = 0, ..., M, n = 0, 1, ...
\end{aligned}$$

For the approximation of $\Delta\phi$ a second or a fourth order finite difference scheme is used. A numerical comparison of both methods is presented in part IV.
The generalization to $d = 2, 3$ is straightforward using tensor products.

7.1 Computational Remarks

BEFD is a very powerful tool for discretizing the gradient flow (4.1.1) – (4.1.3) (see [BT09]). It is unconditionally stable. In terms of accuracy it satisfies a first order accuracy in time $\mathcal{O}(k)$ and a second or fourth order accuracy in space, i.e. $\mathcal{O}(h^2)$ and $\mathcal{O}(h^4)$ respectively. As explained in chapter 3, the exponential decay of the groundstate enables us to impose Dirichlet boundary conditions.
For box potentials it is crucial to choose the width of the box such that the wave function has already decayed to zero sufficiently at the boundary.

For $d = 1$ the memory effort is $\mathcal{O}(M)$, also the runtime scales in $\mathcal{O}(M)$. Obviously, the generalization in $d = 2, 3$ increases both the memory and

runtime to $\mathcal{O}(M^d)$. Therefore, it is favourable to use iterative solvers for higher dimensions than $d = 1$.

For the results in higher dimensions, a *biconjugate gradient stabilized method* (bcgsm) has emerged as favourable. See [VdV92] for detailed theory about bcgsm and [Saa03] for information about iterative solvers for sparse linear systems.

BEFD turns out to be highly usable for ground state computations, since it allows a significantly larger choice of the time step Δt compared to TSSM.

See part IV for detailed comparison of the numerical methods.

Chapter 8

Adaptive Temporal Step Size Adjustment

TSSM as discretization of the normalized gradient flow (see part 4) has many advantages (see chapter 6.3). However, choosing an appropriate time step is crucial to benefit from these advantages.

Reaching a ground state solution requires the minimization of the total energy. Naturally, we request the convergence of the minimization problem to be fast. Though, to obtain a solution satisfying a particular accuracy the time step has to be chosen sufficiently small. Therefore, also an adaptive step size adjustment by for example Richardson Extrapolation (see [BCL07]) does not yield a satisfying solution, since it decreases the time step too fast and increases it afterwards without being close to the exact ground state solution.

For that reason, we provide an approach in which the time step is adaptively decreased. In particular, we start with a comparatively large time step Δt_{init}. Then, the time step is halved, i.e. $\Delta t = \frac{\Delta t}{2}$, every time the solutions at present time t_n and time $t^\star := t_n - \Delta t_{init}$ do not significantly change. Identifying the solution at time $t_n, t^\star$ with ψ^n and $\psi^\star$, forms the following criterion

$$\|\psi^n - \psi^\star\|_{l^2} < \epsilon \tag{8.0.1}$$

where ϵ denotes a particular tolerance.

Note, that the time $t^\star$ is chosen to ensure that (8.0.1) always measures the distance of two solutions with the same temporal distance Δt_{init}. In the algorithm this is guaranteed by line 6 in the pseudo code (see appendix A).

To analyse the convergence, we restrict ourself to the linear case with harmonic oscillator potential such that there is an exact ground state solution ψ. We measure the error as the relative l^2 norm distance (see (9.1.3)). Here, the numerical approximations ψ^n are obtained by applying different time step strategies.

However, choosing a small tolerance ϵ is not sufficient to obtain a fast

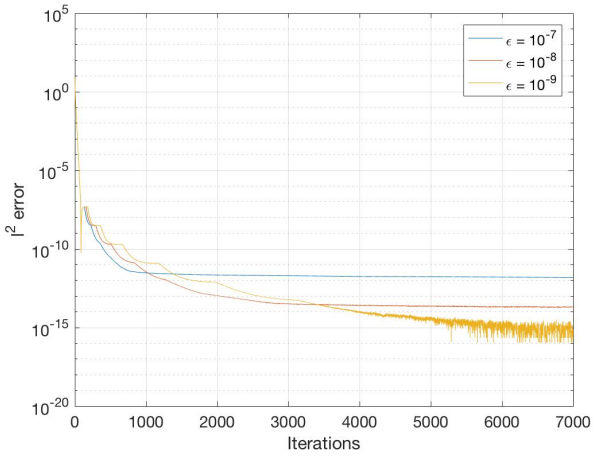

(a) *Relative* l^2 *error with different tolerances* ϵ

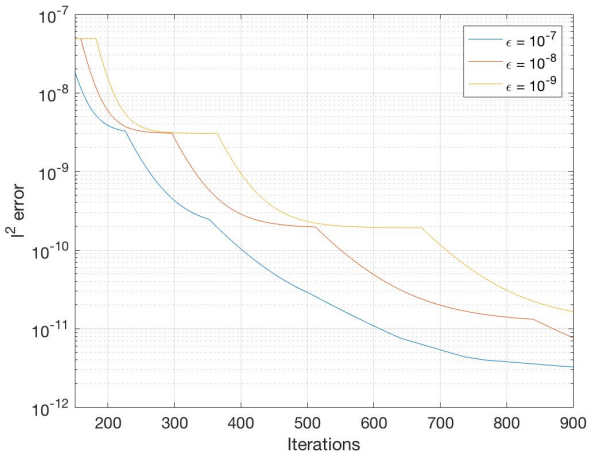

(b) *Zoomed in for Iterations in the beginning*

Figure 8.1

and accurate convergence. Figure 8.1a gives evidence that choosing a smaller tolerance ($\epsilon = 10^{-9}$) yields machine precision. However, in figure 8.1b we observe that in the beginning methods with larger tolerance ϵ produce more accurate solutions. The tolerance picks the time at which the time step is halved. Obviously, this is earlier the case for larger tolerances ϵ. However, as the tolerance is chosen too large ($\epsilon = 10^{-8}$ or $\epsilon = 10^{-7}$) in figure 8.1b, the obtained accuracy in the end is bounded (around 10^{-12} in figure 8.1b).

To improve the results of 8.1b the tolerance is also adaptively chosen. In

particular, we choose

$$\epsilon_0 = \epsilon_{init} \tag{8.0.2}$$

$$\epsilon_{i+1} = \left(\frac{\epsilon_i}{2}\right) \tag{8.0.3}$$

with an initial tolerance ϵ_{init}. The index i is increased to $i+1$ when the criterion (8.0.1) is satisfied with ϵ_i, i.e. when the time step is halved (see appendix A).

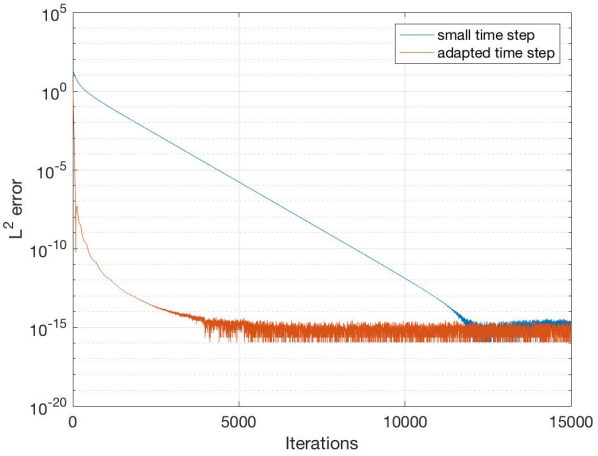

(a) *Relative l^2 error with and without adaptive step size control*

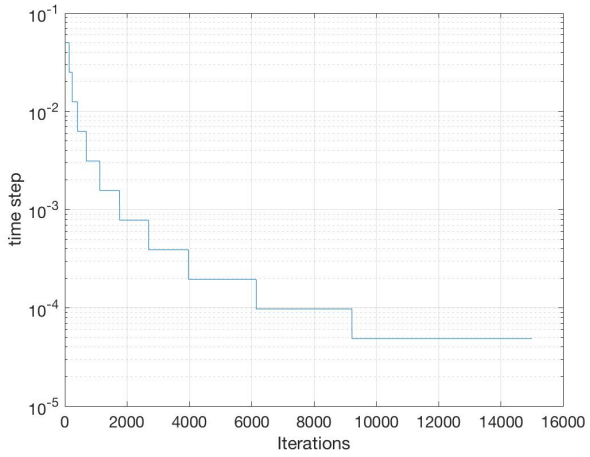

(b) *Associated time step size*

Figure 8.2

Following this approach, figure 8.2a displays the l^2 error for $\epsilon_{init} = 10^{-7}$,

$\Delta t_{init} = 0.05$. This choice yields machine accuracy after only 4000 Iterations. The blue curve in 8.2a shows the convergence for a fixed time step $\Delta t = 0.0001$. We observe, that the convergence is significantly slower than in the adaptive case.

Figure 8.2b shows the times when Δt is decreased according to the Iterations.

Part IV

Numerical Results

Chapter 9

Comparison of Different Numerical Methods

In this chapter, we compare the two methods presented in chapter 6 and 7 with respect to ground state computations and dynamics.

First, the *Quantum Harmonic Oscillator*, i.e. the linear GPE, is used to compare different orders of BEFD and TSSM given the linear Schrödinger equation and an exact solution. Secondly, the nonlinearity constant is slightly increased in order to analyse the numerical behaviour in the nonlinear regime. Finally, we consider dynamics of the GPE and compare the numerical performance and accuracy of BEFD and TSSM.

9.1 Ground States

9.1.1 Comparison in the Linear Case

Quantum Harmonic Oscillator

In order to compare the different numerical methods in an accurate way we need ¨exact solution¨.

Consider the Hamiltonian operator with quantum harmonic oscillator as potential

$$H = \frac{-\hbar^2}{2m}\Delta + \frac{1}{2}m\omega^2 x^2$$

with m, k, w as atomic mass, force constant and angular frequency. Notethat this corresponds to the GPE for $\lambda = 0$, i.e. without nonlinearity.

The time-independent Schrödinger equation can then be written as

$$H\psi = E\psi$$

and is explicitly solved by the stationary states

$$\psi_n(x) = \left(\frac{m\omega}{\pi\hbar}\right)^{\frac{1}{4}} \frac{1}{\sqrt{2^n n}} H_n\left(\frac{m\omega}{\hbar}x\right) e^{-\frac{m\omega x^2}{2\hbar}}$$

where H_n denote the so called *Hermite polynomials*. These stationary states can either be derived by an analytical method using *power series* or by an algebraic approach using *ladder operators*. For a detailed derivation see [GS18].

The ground state solution ($n = 0$) can be expressed as

$$\psi_0(x) = \left(\frac{m\omega}{\pi\hbar}\right)^{\frac{1}{4}} e^{-\frac{m\omega x^2}{2\hbar}} \tag{9.1.1}$$

Note, that in the dimensionless form of the GPE (see chapter 1) $\hbar = 1, m = 1, \omega = 1$.
This gives the formal ground state solution

$$\psi_0(x) = \left(\frac{1}{\pi}\right)^{\frac{1}{4}} e^{-\frac{x^2}{2}} \tag{9.1.2}$$

Results

(9.1.2) enables us to establish an error analysis given an exact solution ψ and a numerical approximation ψ^n at discrete time $t = t_n$.

The error is measured by the distance between ψ and ψ^n in the relative l^2 norm

$$e(t_n) := \frac{\|\psi - \psi^n\|_{l^2}}{\|\psi\|_{l^2}}, \quad n \geqslant 0 \tag{9.1.3}$$

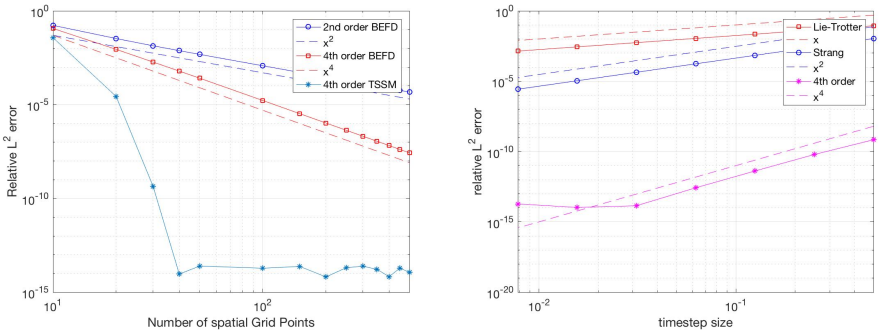

(a) (b)

Figure 9.1: *Numerically observed convergence orders of TSSM and BEFD for the quantum harmonic oscillator, a) spatial, b) temporal*

Figure 9.1a illustrates the error (9.1.3) for an approximation ψ^n with respectively $M = 10, ..., 500$ grid points. Choosing $\Delta t = 0.001$ as initial time step

and decreasing it monotonously (see chapter 8) guarantees a negligible time discretization error. These results are in good agreement with the theoretical **spatial** orders of the considered methods:

- BEFD with a second order finite difference discretization in space
- BEFD with a fourth order finite difference discretization in space
- TSSM with a spectral discretization in space

The slopes of the dashed lines represent the expected theoretical order.
Figure 9.1b displays the numerically observed **temporal** convergence order of different splitting methods. Lie-Trotter satisfies a first order splitting, Strang a symmetric second order splitting and the splitting (6.2.4) is a fourth order scheme. For a more detailed convergence analysis see [NT09, Tha12].

9.1.2 Comparison in the Nonlinear Case

In this section we take a small nonlinearity constant and investigate whether the results from the linear case remain valid.

In order to illustrate the accuracy of different methods a reference function is required. Since analytically there is no exact solution for most of the initial value problems, we use the ground state solution ψ computed by the fourth order TSSM (6.2.4) with a very small time step and a fine mesh (1024×1024).

Moreover, let μ be the corresponding exact eigenvalue of the nonlinear eigenvalue problem of chapter 3. In the following let ψ^n and μ^n be respectively the numerical approximation of ψ and μ at time t_n.

We slightly increase the nonlinearity from the linear equation ($\lambda = 0$) to $\lambda = 3$.

Once the exact solution with 1024×1024 grid points is computed, a numerical approximation ψ^n with respectively $M = 10, ..., 200$ grid points is determined. The error is then measured by

$$e_\mu(t_n) := \frac{|\mu - \mu^n|}{|\mu|} \tag{9.1.4}$$

for the spatial convergence analysis and by (9.1.3) for the temporal convergence analysis.

The results displayed in figure 9.2a visualize the numerically observed **spatial accuracy** of a second and a fourth order finite difference discretization, as well as a TSSM (with spectral accuracy), for a nondimensionalized harmonic oscillator as confining potential

$$V(x) = \frac{x^2}{2}, \quad x \in [-4, 4]$$

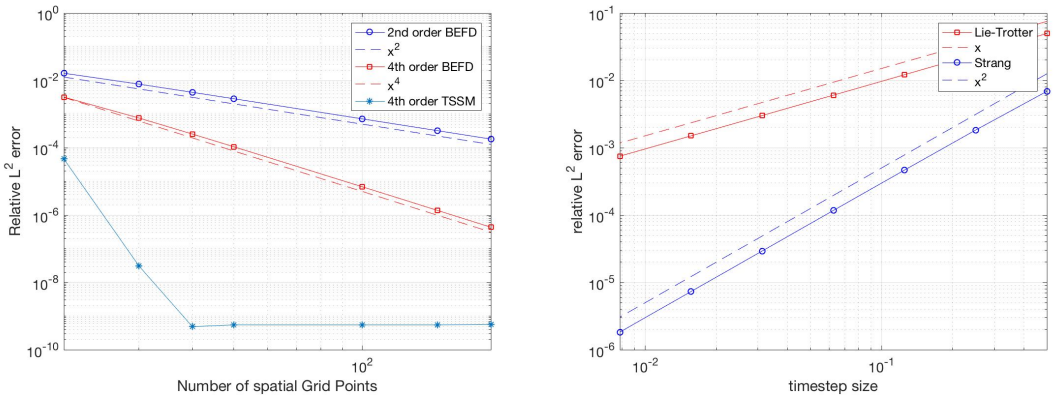

(a) (b)

Figure 9.2: *Numerically observed convergence orders of TSSM and BEFD for the nonlinear Schrödinger equation*

Further, the error obtained by the **operator splitting** is observed in figure 9.2b for Lie-Trotter and Strang splitting. Again, the slopes of the dashed lines reflect the expected theoretical order.

Although, an analytical solution is not provided in the nonlinear equation, we can conclude that the results of the linear case generalize to the nonlinear regime if the nonlinearity is slightly increased. [NT09, TCN09] provide a detailed convergence analysis of splitting methods.

9.2 Dynamics

Regarding real time propagation only TSSM is used. BEFD has advantages only for ground states.

The data in figure 9.3 is produced by using the 4th order splitting (6.2.4) to obtain an exact wave function. We fix a time $t^\star = 1$ until which the time is propagated for the following initial data:

$$\psi_0(x) = \frac{1}{\pi^{1/4}} e^{-\frac{x^2}{2}}$$

Then we compare the wavefunction of the 4th order splitting to a Strang splitting and compute the error by (9.1.3).

In particular, for the spatial error we choose a small time step such that the temporal error is negligible and a fine mesh (1024x1024) to obtain the exact solution ψ. Then we compute a numerical approximation ψ^n with $M = 8, 16, 32, 64, 128, 256$ (see 9.3a).

For the temporal error we compute an exact ground state solution using the TSSM of 4th order. Plugging this ground state solution into the equation and

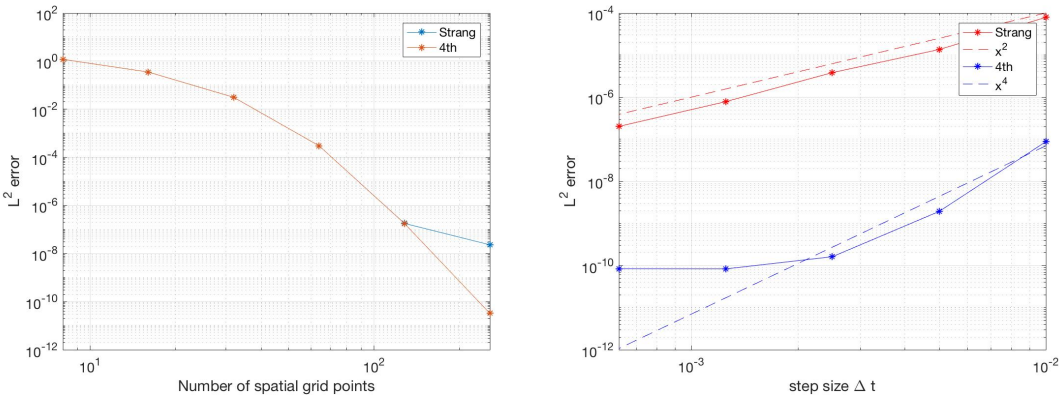

(a) (b)

Figure 9.3: *Strang splitting error, a) spatial, b) temporal*

propagate time we expect the density to remain unchanged. We compute ψ^n for $\Delta t = 0.01, 0.005, 0.0025, 0.00125, 0.000625$ to numerically obtain the temporal error (figure 9.3b). The error curve is in agreement with the second and 4th order accuracy of TSSM in time.

Chapter 10

Investigation of Box Parameters

In this chapter, we illustrate numerical behaviour of confinement with box potentials. As stated in chapter 2, a smoothing of discontinuities is required to apply TSSMs because of the global evaluation of Fourier transforms in space.

The degree of smoothing depends on several parameters:

- Box Parameters
  - Layer size $1/d$ (see figure 10.1a and 2.1b)
  - Height h of the box (see figure 10.1b and 2.1a)
- Equation Parameter
  - Nonlinearity constant λ in (1.1.3) (see figure 10.1c)

These parameters determine both the smoothness of a box potential and its corresponding ground state solution, which gives evidence to investigate these parameters with respect to the required number of grid points M. In the following two sections we examine these parameters for ground state computations as well as dynamics.

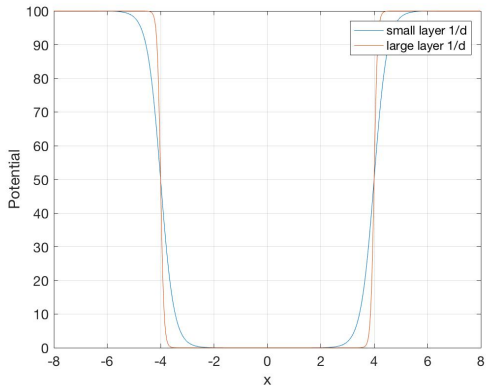

(a)

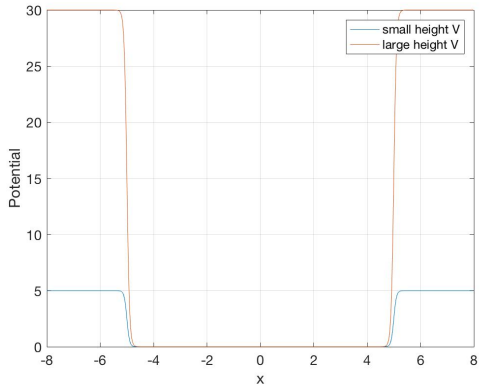

(b)

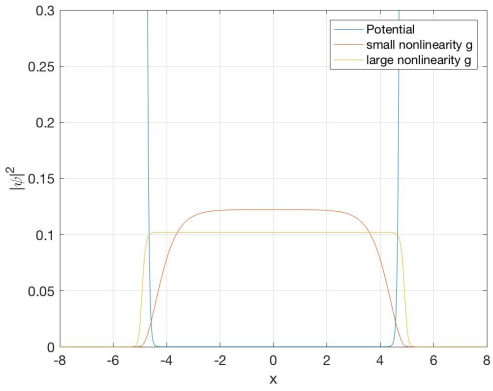

(c)

Figure 10.1: *Parameters defining a Box Potential*

10.1 Ground States

To determine a reference function ψ as ¨exact ground state¨ solution we use again a fourth order TSSM (see (6.2.4)) with a small time step. We apply the adaptive temporal step size adjustment from chapter 8 and a very fine mesh of 1024.

The error is measured by (9.1.4) where μ is the exact eigenvalue and μ^n the corresponding approximated eigenvalue at time $t = t_n$.

In the following, approximations ψ^n with different spatial resolutions are computed by a TSSM with Strang splitting and BEFD (4th order in space).

The results in figures 10.2a, 10.2b display the required spatial resolution with respect to a varying size of the layer. The smaller d, the smoother are the potential edges. Layer sizes of $1/d = 2, ..., 16$ are investigated. We can conclude that with increasing d more grid points are required to obtain an accurate ground state solution, both for TSSM and BEFD.
Furthermore, we technically observe two results. On the one hand, we obtain for one fixed layer size d higher accuracy the larger the resolution is. On the other hand, for a fixed resolution the choice of a small d yields more accurate solutions (except for some outliers for resolutions 128 and 256).
Another interesting issue to observe is that TSSM reaches errors in the scale of $10^{-8} - 10^{-10}$, whereas BEFD produces errors in the scale of $10^{-6} - 10^{-7}$. The reason for that is the spectral vs. a 4th order accuracy of TSSM and BEFD respectively in space, see chapter 9.

The results from figures 10.2c and 10.2d display highly interesting insights. One could expect a large influence of the height on the numerical results, but we barely observe it. Whereas the size of the layer d clearly determines the required resolution, the height does not. Irrespective of the number of grid points, the error does not significantly increase if the box is heightened. 10.2c displays this result for TSSM and 10.2d for BEFD. Hence, this is not only observed for a single numerical method.
Nevertheless, for a fixed height h we observe lower errors if the number of grid points is increased.

However, figures 10.2e, 10.2f support our intuition about the choice of λ. The higher λ is chosen, the sharper is the wave function of the ground state solution, see figure 10.1c.
Figures 10.2e and 10.2f reveal two intuitive results. Firstly, for a fixed resolution the error increases as the nonlinearity constant increases. Secondly, if we fix a particular constant λ we can conclude that for both methods a higher resolution yields a smaller error and therefore a more accurate solution.
A crucial condition to compute stationary states with high nonlinearities λ is a box with a sufficiently large height. As the nonlinearity constant increases, the condensate expands more and more. However, we want the wave function to decay to zero as x approaches the boundary. Therefore, a stronger confinement is required as the nonlinearity constant gets larger.

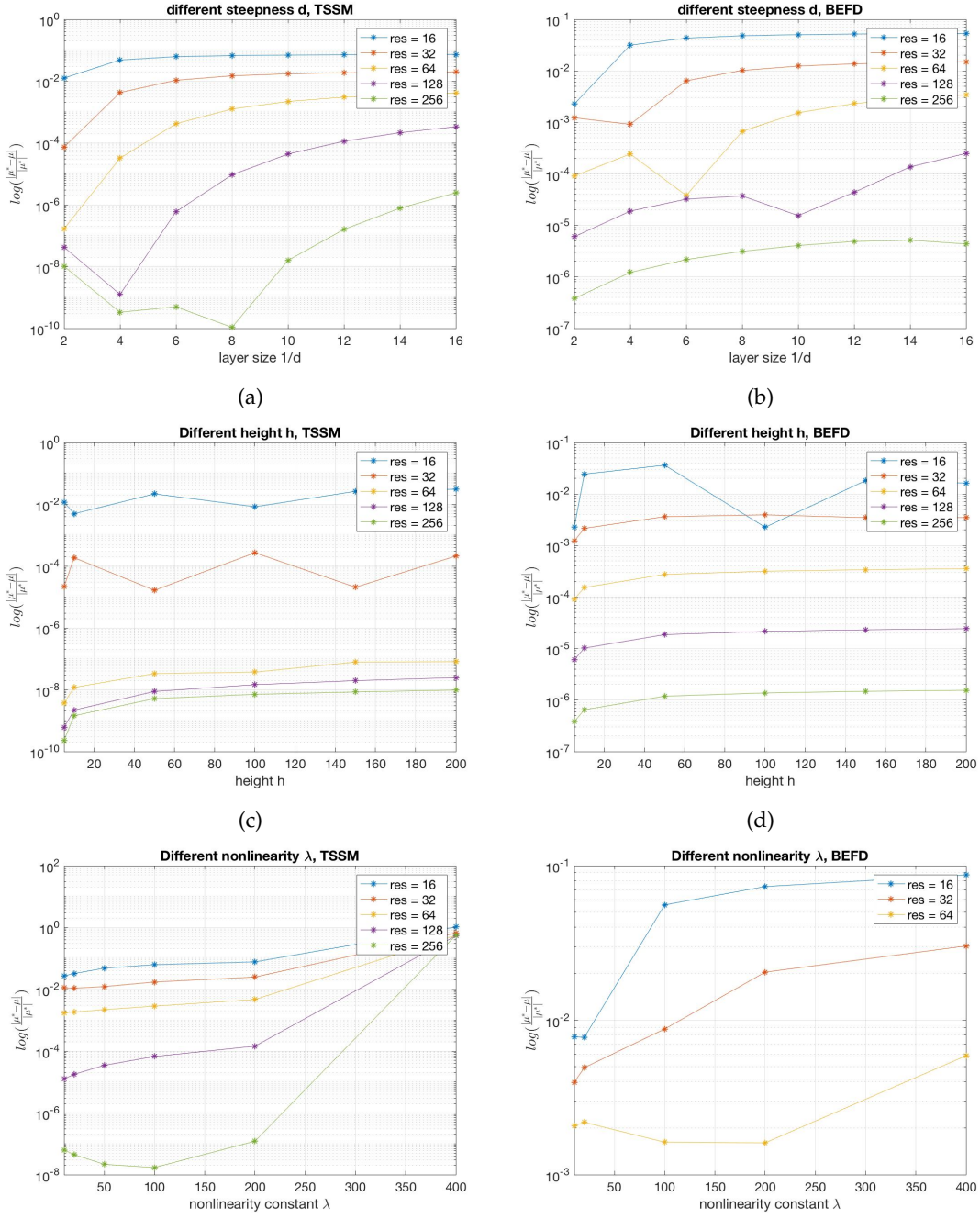

Figure 10.2: *Numerically observed performance and accuracy analysis of box parameters for ground state computations: left: TSSM, right: BEFD*

10.2 Dynamics

As in the previous chapter we investigate the influence of the box parameters $1/d, h$ an the equation parameter λ on the required number of grid points. In this chapter, the focus lies on evolutionary time dependent computations.

As reference function we choose a function ψ computed by a 4th order TSSM (see (6.2.4)) with a Gaussian as initial data

$$\psi_0(x) = \frac{1}{\pi^{1/4}} e^{-\frac{x^2}{2}}$$

We propagate until a certain time $t^\star$ and compare $\psi(0, t^\star)$ with the approximation $\psi^n(0, t^\star)$ where n here is the required number of iterations to reach the time $t^\star$. ψ^n is obtained by propagating a TSSM with Strang splitting for varying number of grid points.

The error is then measured by

$$e(t_n) := |\psi(0, t^\star) - \psi^n(0, t^\star)| \tag{10.2.1}$$

Overall, we obtain similar results as in the stationary case.
Beginning with figure 10.3a, we observe two interesting results. Firstly, for a fixed layer size $1/d$ a higher resolution yields smaller errors, which is in agreement with the intuition. Moreover, we observe smaller errors for smaller ds, irrespective of the resolution. Since the choice of a large d produces very sharp edges of the box potential, this also matches the intuition.
Furthermore, we need to emphasize that the influence of d on the accuracy seems to be very large. For the highest resolution of 256 grid points the error scales from 10^{-14} for a small d to only 10^{-5} for a large d.

Unlike the layer size, the height does not have as much influence on the accuracy (see figure 10.3b). We observe almost the same error for all investigated resolutions and varying heights h. For higher boxes we expect larger errors, since the height of box potentials determines the steepness of the box barriers. However, the stronger confinement for higher boxes does not imply larger errors.
However, as we expect, higher resolutions exhibit smaller errors for a fixed height h.

Regarding the nonlinearity constant λ figure 10.3c yields the expected results. As the nonlinearity increases, the error to the exact solution increases simultaneously. The choice of λ seems to have a large impact on the numerical accuracy. For a resolution of 128 a small λ produces an error of around 10^{-8} whereas for $\lambda = 200$ we observe an error of around 10^{-1}.

We conclude that for both ground state computations as well as dynamics the size of the layer d and the nonlinearity constant λ require a specific numerical treatment. In fact, the number of grid points should be increased in these cases. Note, that due to the nondimensionalization of chapter 1 λ includes the number of atoms N, i.e. for many atoms a higher resolution is required.

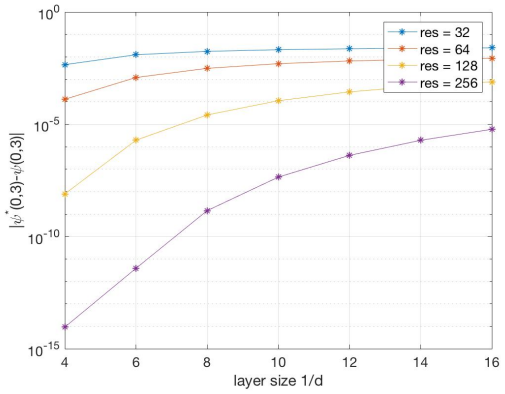

(a)

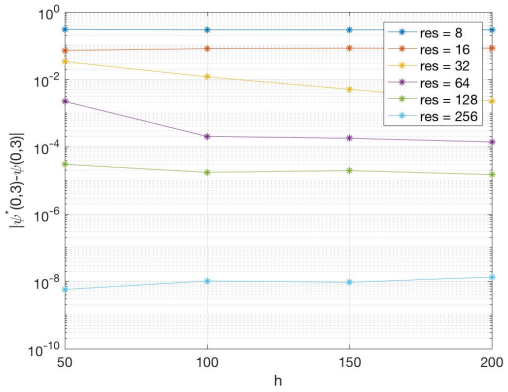

(b)

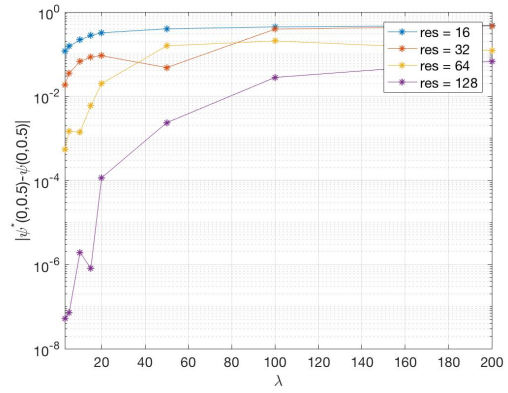

(c)

Figure 10.3: *Numerically observed accuracy analysis of TSSM for time propagation of box parameters*

10.3 Comparison of Confining Potentials – Harmonic Oscillator vs. Box Potential

As the previous two sections investigated the influence of the parameters defining a box potential, the following study will compare the time evolution in a confinement with a harmonic oscillator vs. a box potential. We perform dynamics for a condensate with initial data

$$\psi_0(x) = \frac{1}{\pi^{1/4}} e^{-\frac{x^2}{2}} e^{ik_0 x} \tag{10.3.1}$$

which represents a wave packet localized at the origin.
The GPE is solved by the 4th order splitting scheme (6.2.4) on the domain $\Omega = [-8, 8]$ with a resolution of 512. $\Delta t = 0.001$, $k_0 = 3$ and as nonlinearity constant $\lambda = 3$ is chosen. The box potential has a layer size of $1/d = 4$ and a height of $h = 5$.

Figure 10.4 displays the time evolution of the wave packet (10.3.1) for a harmonic oscillator (left) as well as a box potential (right) as confining potential. In particular, the initial wave packet (see figures 10.4a and 10.4b) moves with a certain group velocity to the boundary and is reflected at the confining potential respectively. In figures 10.4c and 10.4d we see the density function at time $t = 3$. In the case of a harmonic oscillator, the wave packet is reflected the first time at $t = 3$. Even though the wave spreads out, a reflecting wave packet is still observable for the times from $t = 0$ to $t = 9$. For the box potential however the first reflection at the box well (see figure 10.4d) leads to a chaotic behaviour which still holds for later times (see figures 10.4f and 10.4h).

These observations underline the importance of a particular numerical treatment of box potentials (see chapter 10). Even though, the layer size, the height and the nonlinearity constant are chosen relatively small the first reflection at the potential well leads to a chaotic behaviour.

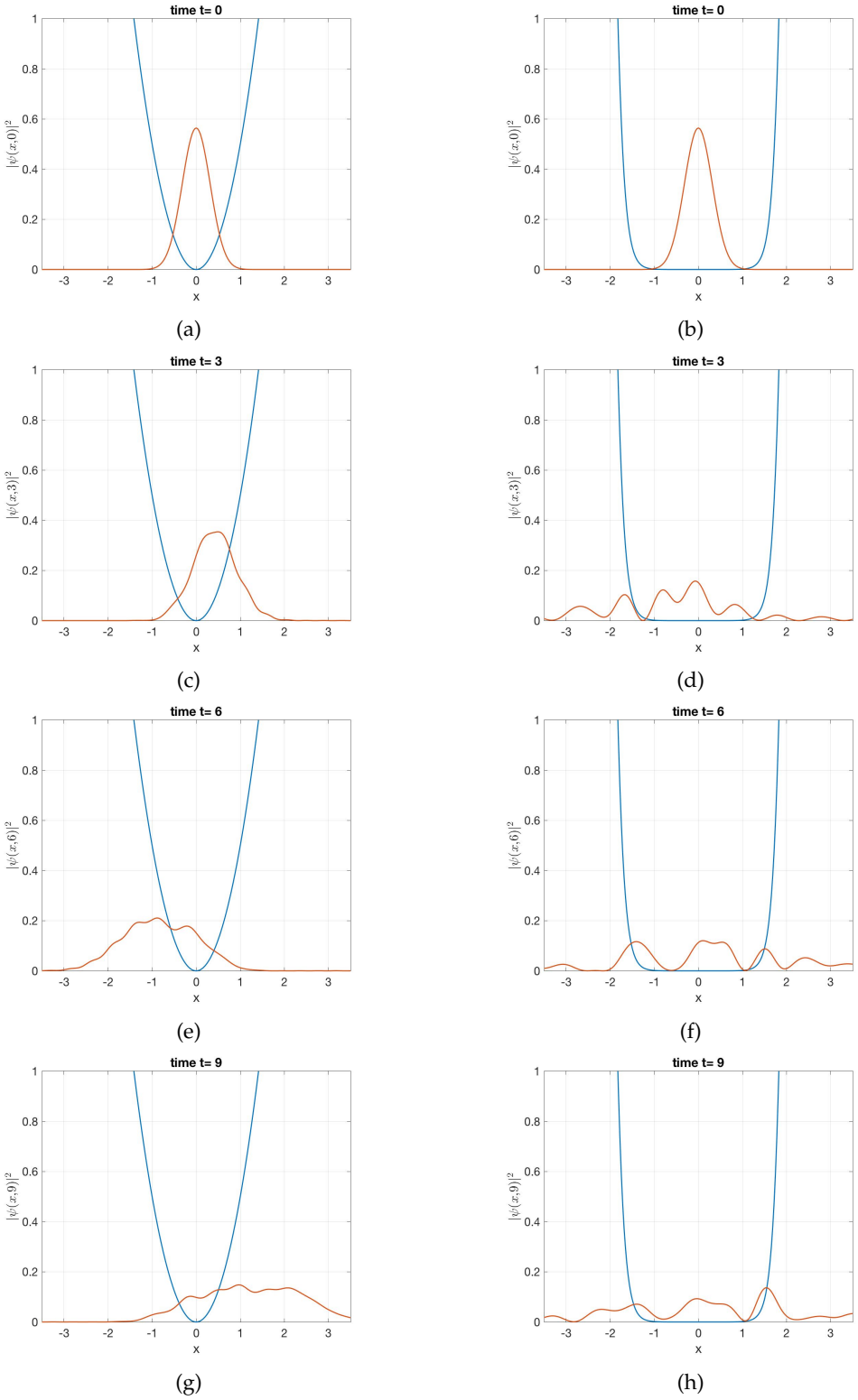

Figure 10.4: *Travelling wave packet confined by a harmonic oscillator (left) and a box potential (right)*

Chapter 11

Higher Space Dimensions

11.1 2D Examples

11.1.1 Ground State Applications

In this chapter, a ground state solution in two dimensions ($d = 2$ in (1.1.3)) is computed using TSSM with Strang splitting and adaptive temporal step size adjustment (see chapter 8).
As external potential we choose a smoothed box potential in both directions x and y, i.e.

$$V_x = h * \frac{\tanh(\frac{1}{d} * (|x| - \frac{w_x}{2.0})) + 1.0)}{2} \tag{11.1.1}$$

$$V_y = h * \frac{\tanh(\frac{1}{d} * (|y| - \frac{w_y}{2.0})) + 1.0)}{2} \tag{11.1.2}$$

with $w_x, w_y = 6$ as width of the smoothed box, $d = 10$ as size of the layer and $h = 100$ as height.

The equation is solved on the domain $\Omega = [-8, 8] \times [-6, 6]$ with a resolution of 128 on each interval for the spectral method. As initial time step $\Delta t = 0.001$ is chosen, however Δt is adaptively decreased (see chapter 8).

Figure 11.1a shows the wave function density with slices along $y = 0$ and $x = 0$ respectively for two nonlinearity constants $\lambda = 20, 200$.

In figures 11.1b and 11.1c again the wave function density is displayed as heat map. The sharp edges are observed for the large nonlinearity constant $\lambda = 200$ (see 11.1c). For a more detailed analysis of the influence of box parameters and the nonlinearity constant on the solution see chapter 10.

11.1.2 Dynamics

In order to illustrate the time evolution of the wave function in two dimensions, we consider the domain $\Omega = [-8, 8] \times [-6, 6]$ the same external potential as

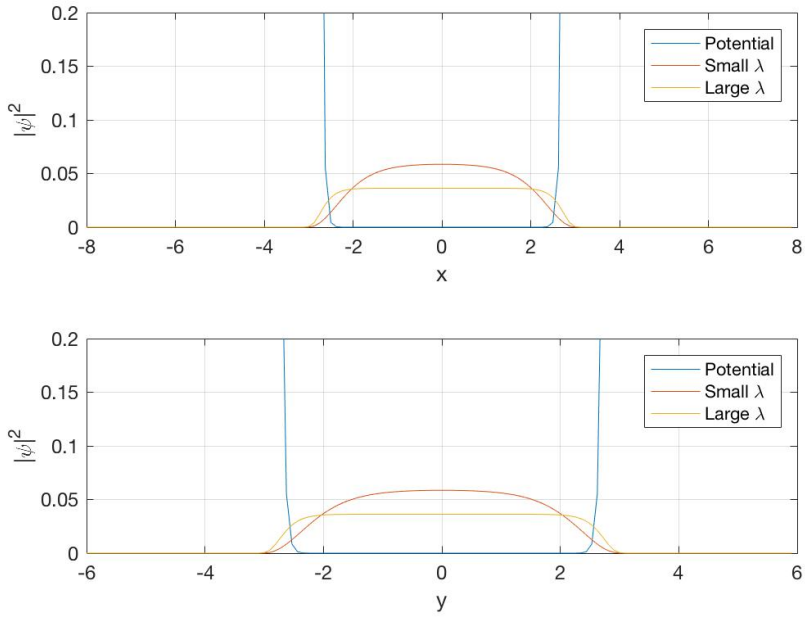

(a) *Slice along* $y = 0$ *and* $x = 0$ *respectively*

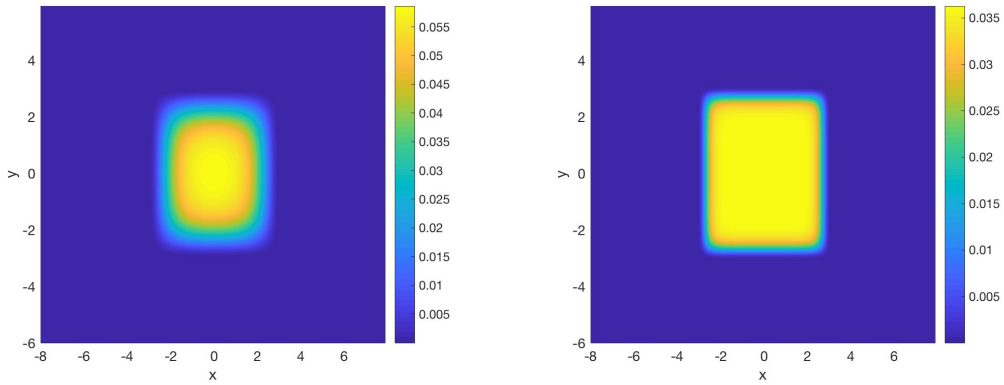

(b) *Small* $\lambda = 20$ (c) *Large* $\lambda = 200$

Figure 11.1: *Ground State solution for small and large nonlinearity constant* λ

before ((11.1.1)-(11.1.2)) and

$$\phi_0(x,y) = \frac{(\gamma_x\gamma_y)^{1/4}}{\pi^{1/2}} e^{-(\gamma_x x^2+\gamma_y y^2)/2} \tag{11.1.3}$$

as initial data with $\gamma_x, \gamma_y = 1$.

The nonlinearity constant is fixed to $\lambda = 20$.

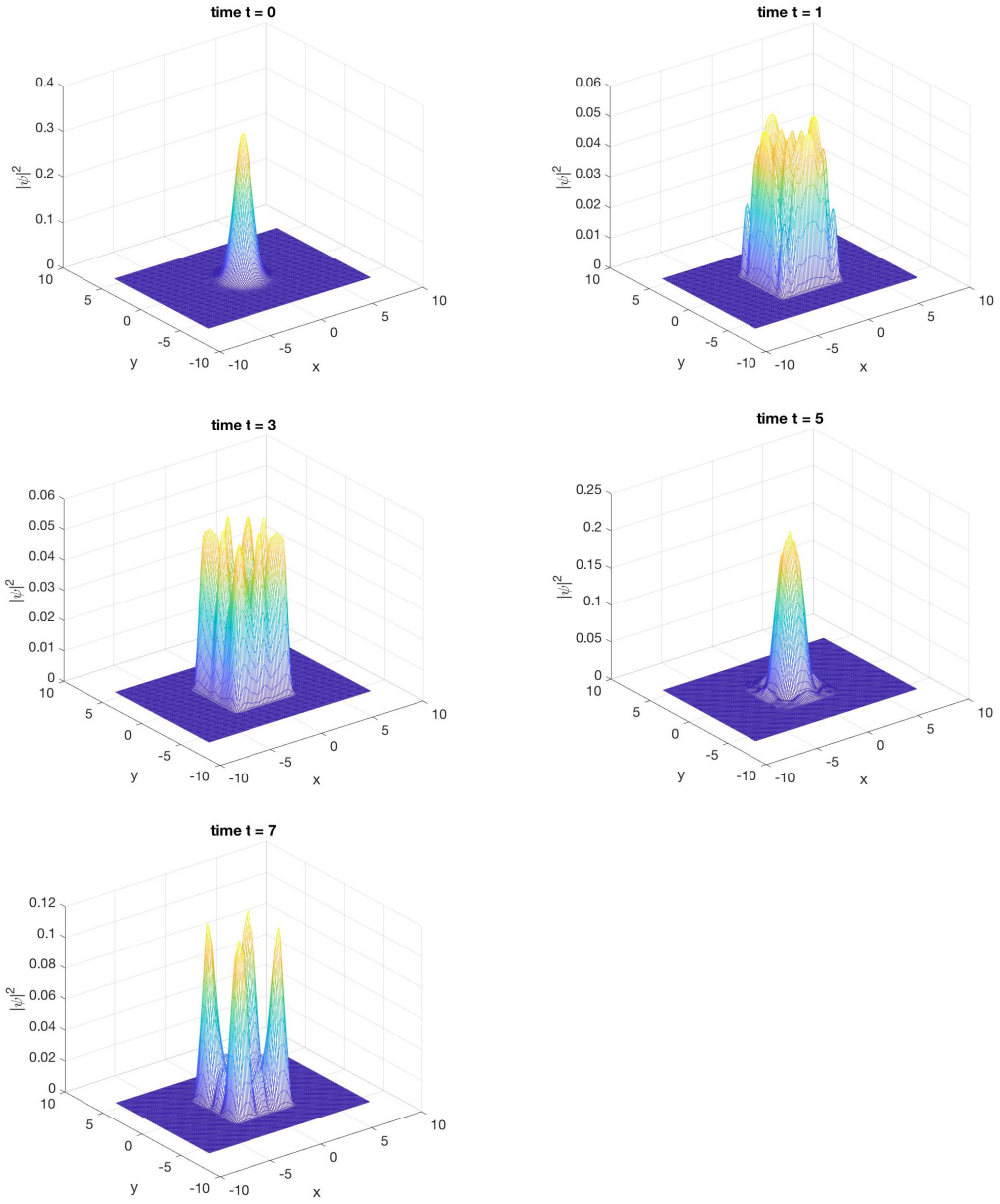

Figure 11.2: *Wave Function Density for* $\lambda = 20$ *in Box Potential up to a final time* $T = 7$

Figure 11.2 displays the time integration of the GPE at different times

$T = 0, 1, 3, 5, 7$ using TSSM with Strang splitting.

11.2 3D Examples

11.2.1 Ground State Applications

A ground state solution in three dimensions ($d = 3$ in (1.1.3)) is computed by the fourth order TSSM scheme (6.2.4) with the box potential defined by means of the functions

$$V_x = h * \frac{\tanh(\frac{1}{d} * (|x| - \frac{w_x}{2.0})) + 1.0)}{2} \tag{11.2.1}$$

$$V_y = h * \frac{\tanh(\frac{1}{d} * (|y| - \frac{w_y}{2.0})) + 1.0)}{2} \tag{11.2.2}$$

$$V_z = h * \frac{\tanh(\frac{1}{d} * (|z| - \frac{w_z}{2.0})) + 1.0)}{2} \tag{11.2.3}$$

where $w_x, w_y, w_z = 6$ denotes the width of the smoothed box, $d = 10$ the layer size and $h = 100$ the height of the box.

The gradient flow is solved on the domain $\Omega = [-8, 8] \times [-8, 8] \times [-6, 6]$ with a resolution of 64 on each interval. As initial time step $k = 0.001$ is chosen, however it is adaptively reduced by the method of chapter 8.

As in chapter 11.1 a ground state solution for two different nonlinearity constants is computed. First $\lambda = 50$, whereas the second solution is generated by $\lambda = 500$.

Figure 11.3 displays the two observed wave function densities as well as the smoothed box potential. As in the 2d example, the influence of λ can be clearly observed in the solutions .

11.2.2 Dynamics

Time Integration in 3d is investigated by applying the fourth order TSSM on the GPE. As initial data we choose

$$\phi_0(x, y) = \frac{(\gamma_x \gamma_y \gamma_z)^{1/4}}{\pi^{3/4}} e^{-(\gamma_x x^2 + \gamma_y y^2 + \gamma_z z^2)/2} \tag{11.2.4}$$

with $\gamma_x, \gamma_y, \gamma_z = 1$. Time is propagated on the domain $\Omega = [-8, 8] \times [-6, 6] \times [-6, 6]$ with $M = 128$ grid points. $\Delta t = 0.001$, $g = 50$ and we choose the potential consisting of (11.2.1) – (11.2.3). The results in figure 11.4 display the density of the wave function at times $T = 0, 1, 3, 5, 7$.

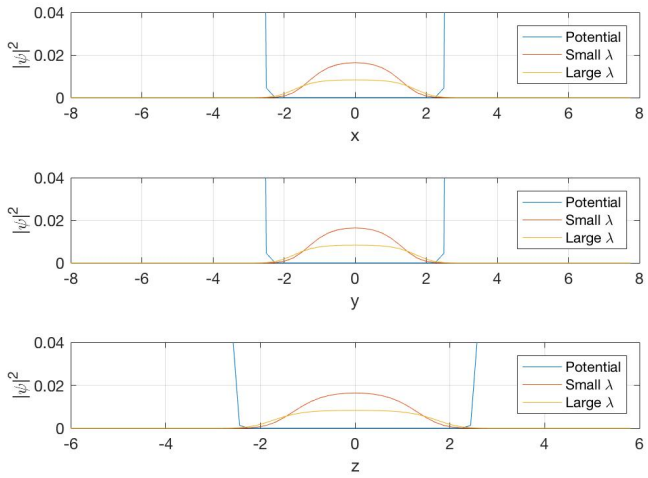

Figure 11.3: *Ground State solution for small and large nonlinearity constant* λ *slice along* $y, z = 0$, $x, z = 0$ *and* $x, y = 0$ *respectively*

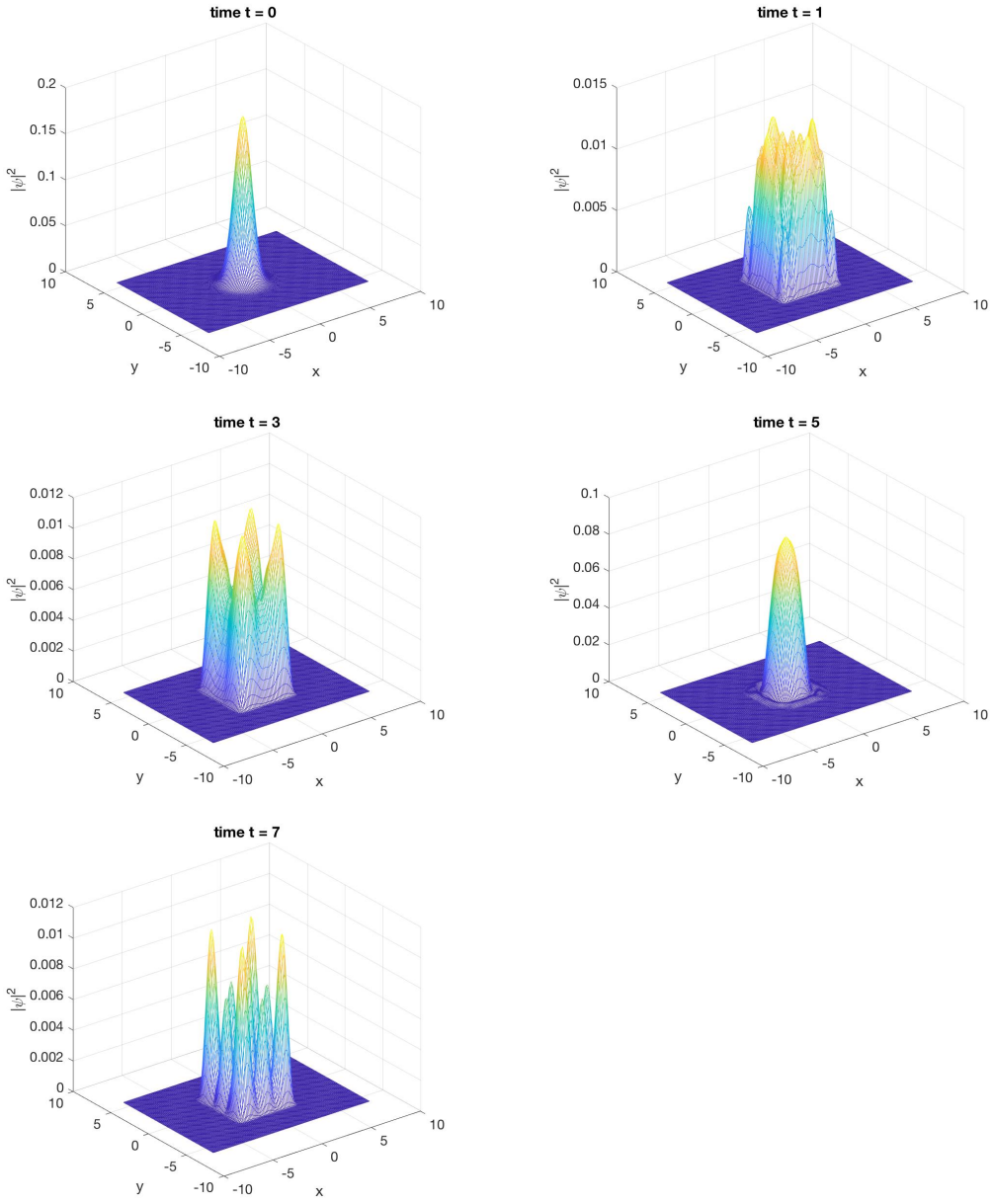

Figure 11.4: *Density of the wave function for* $\lambda = 50$ *in Box Potential up to a final time* $T = 7$*, slice along* $z = 0$

Chapter 12

Implementation Details

All of the presented results were generated by programs written in MATLAB and executed on the following devices (CPUs and GPUs):

- Intel Core i7-4770K CPU @ 3.5GHz x 8: 4 Cores, 8 Threads
- GeForce GTX TITAN: 2688 CUDA Cores

The time measurements were obtained using the measurement tool *tic toc* of MATLAB.

Regarding the runtime of TSSM per time step we obtain $\mathcal{O}(M^d \log M)$ for M denoting the spatial resolution (see chapter 6.2). In spite of the *FFT* operation (which is done for the free part of the equation, see chapter 5.2) is enormously reducing the computational costs, long runtimes for higher dimensions ($d \geqslant 1$) are still observed on the CPU. Due to their highly parallel architecture, GPU

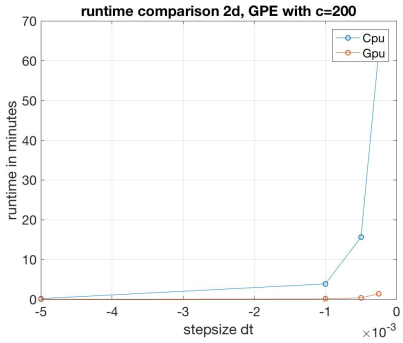

Figure 12.1: Runtime for Example 2 on GPU and CPU for step sizes dt= [0.005, 0.001, 0.0005, 0.00025]

devices are very suitable for this kind of numerical computation. Unlike CPUs,

a GPU can execute several hundred threads simultaneously, which is very favourable for highly parallel algorithms such as the *FFT* operation.

It turns out, that running the algorithm on a GPU for dimensions $d = 2, 3$ is very efficient. Figure 12.1 displays this result. It compares the runtime on a CPU and a GPU for different time steps Δt in two dimensions. For the smallest step size of $\Delta t = 0.00025$ the CPU requires around 62.3 minutes, whereas the GPU only needs approximately 1.3 minutes.

Part V

The end

Chapter 13

Conclusion and Outlook

13.1 Conclusion

In this thesis we have presented numerical methods for the Gross-Pitaevskii equation with a particular focus on numerical treatment for a confinement with a box potential. A second and fourth order time splitting spectral method (order w.r.t. time) has been considered and compared to a second and fourth order backward Euler finite difference scheme (order w.r.t. space). For these methods, parameters describing a box potential have been investigated. It has been established that especially the choice of the layer size d and the nonlinearity constant λ requires a fine spatial mesh. However, against expectation the height of a box potential does not influence the accuracy as much as the other two parameters.

Moreover, an approach for obtaining a particularly precise ground state solution by dynamically decreasing the temporal step size was established. We decrease the time step as a solution does not significantly change over a particular time. The tolerance between two solutions has also been adaptively decreased such that we observe an accurate solution in very few iterations.

In order to confirm the presented theory, numerical experiments generated by a MATLAB implementation and executed on a GPU (for higher dimensions) have been studied.

13.2 Outlook

As part of this research area is becoming an ever more interdisciplinary research field, there are still many important issues to be addressed. For example, one of them is developing an algorithm guaranteeing en even faster convergence of ground state solutions by cleverly adapting the imaginary time step. An algorithm which optimizes the parameters of chapter 8 would probably converge even faster to an accurate solution. However, the choice of the parameters

seems to be highly dependent on the particular problem, which complicates an automatic choice of criterion parameters. Furthermore, establishing an optimal stopping criterion for these ground state computations is an interesting open question, since in most cases analytical solutions do not exist.

Considering experimentally obtained external potentials in computational methods is another challenging task. The investigation of accurate methods to deal with box potential is not the only interesting challenge. Also other experimentally observed potentials can be numerically examined.

Regarding computational efficiency the development of novel computer architectures induces the design of new programming languages with a particular focus on parallelism. Together, this trend improves computational capacity as well as user friendliness. Also in the context of Gross-Pitaevskii type equations this development will offer new opportunities.

Appendices

Appendix A

Adaptive Temporal Step Size Adjustment – Algorithm

Define $err = \|\psi^n - \psi^{n-1}\|_{l^2}$ as the error of a solution at time t_n and a solution at time t_{n-1}. The following algorithm describes the strategy to decrease the time step during the ground state computation explained in chapter 8.

$\epsilon = \epsilon_{init}$;
$\psi_{old} = \psi$;
for $i \leftarrow 0$ **to** *maxIterations* **do**
    Compute new ψ;
    $count = 0$;
    if $mod(i, 2^{count}) == 0$ **then**
        $err = \|\psi^n - \psi^{n-1}\|_{l^2}$;
        if $err < \epsilon/(2^{count})$ **then**
            $\Delta t = \frac{\Delta t}{2}$;
            count++;
        end
        $\psi_{old} = \psi$;
    end
end

Bibliography

[ABB13] Xavier Antoine, Weizhu Bao, and Christophe Besse. Computational methods for the dynamics of the nonlinear Schrödinger/Gross-Pitaevskii equations. *Computer Physics Communications*, 184:2621–2633, 12 2013.

[AD14] Xavier Antoine and Romain Duboscq. Robust and Efficient Preconditioned Krylov Spectral Solvers for Computing the Ground States of Fast Rotating and Strongly Interacting Bose-Einstein Condensates. *J. Comput. Phys.*, 258(C):509–523, February 2014.

[AEM+95] M. H. Anderson, J. R. Ensher, M. R. Matthews, C. E. Wieman, and E. A. Cornell. Observation of Bose-Einstein Condensation in a Dilute Atomic Vapor. *Science*, 269(5221):198–201, 1995.

[BC12] Weizhu Bao and Yongyong Cai. Mathematical theory and numerical methods for Bose-Einstein condensation. *Kinetic and Related Models*, 6, 12 2012.

[BCL07] Benjamin Belfort, Jérôme Carrayrou, and F Lehmann. Implementation of Richardson extrapolation in an efficient adaptive time stepping method: Applications to reactive transport and unsaturated flow in porous media. *Transport in Porous Media*, 69:123–138, 06 2007.

[BD04] Weizhu Bao and Qiang Du. Computing the ground state of the BEC via normalized gradient flow. *Siam Journal on Scientific Computing*, 01 2004.

[BM02] Sergio Blanes and Per Christian Moan. Practical symplectic partitioned Runge Kutta and Runge Kutta Nystrom methods. *Journal of Computational and Applied Mathematics*, 142:313–330, 05 2002.

[Bos24] Bose. Plancks Gesetz und Lichtquantenhypothese. *Zeitschrift für Physik*, 26(1):178–181, Dec 1924.

[BT09] Weizhu Bao and Weijun Tang. Ground-state solution of Bose-Einstein condensate by directly minimizing the energy functional. *Journal of Computational Physics*, 187(1):230 – 254, 2009.

[CW98] Eric A. Cornell and Carl E. Wieman. The Bose-Einstein Condensate. *Scientific American*, 278(3):40–45, 1998.

[DT19] Stéphane Descombes and Mechthild Thalhammer. High-order exponential operator splitting methods for evolutionary problems. A local error expansion and applications to linear Schrödinger equations in the semi-classical regime. 07 2019.

[GS18] David J. Griffiths and Darrell F. Schroeter. *Introduction to Quantum Mechanics*. Cambridge University Press, 3 edition, 2018.

[HLSPSY06] Elliott H. Lieb, Robert Seiringer, Jan Philip Solovej, and Jakob Yngvason. The Mathematics of the Bose Gas and its Condensation. 11 2006.

[JL01] Anthony J. Leggett. Bose-Einstein condensation in the alkali gases: Some fundamental concepts. *Reviews of Modern Physics*, 73:307–356, 04 2001.

[LTE07] Lauri Lehtovaara, Jari Toivanen, and Jussi Eloranta. Solution of time-independent Schrödinger equation by the imaginary time propagation method. *J. Comput. Physics*, 221:148–157, 2007.

[NT09] Christof Neuhauser and Mechthild Thalhammer. On the convergence of splitting methods for linear evolutionary Schrödinger equations involving an unbounded potential. *BIT Numerical Mathematics*, 49:199–215, 03 2009.

[PS04] Lev Pitaevskii and Sandro Stringari. Bose-Einstein Condensation, Oxford University Press, Oxford, 2003. *Journal of Statistical Physics*, 115, 06 2004.

[Saa03] Y. Saad. *Iterative Methods for Sparse Linear Systems*. Society for Industrial and Applied Mathematics, Philadelphia, PA, USA, 2nd edition, 2003.

[Str68] Gilbert Strang. On the Construction and Comparison of Difference Schemes. 1968.

[TCN09] Mechthild Thalhammer, Marco Caliari, and Christof Neuhauser. High-order time-splitting Hermite and Fourier spectral methods. *Journal of Computational Physics*, 228:822–832, 02 2009.

[Tha08] Mechthild Thalhammer. High-Order Exponential Operator Splitting Methods for Time-Dependent Schrödinger Equations. *SIAM J. Numerical Analysis*, 46:2022–2038, 01 2008.

[Tha12] Mechthild Thalhammer. Convergence Analysis of High-Order Time-Splitting Pseudospectral Methods for Nonlinear Schrödinger Equations. *SIAM Journal on Numerical Analysis*, 50:3231–3258, 01 2012.

[Tro59] H. F. Trotter. On the product of semi-groups of operators. *Proceedings of the American Mathematical Society*, 10(4):545–551, 1959.

[VdV92] Henk Van der Vorst. Bi-CGSTAB: A fast and smoothly converging variant of Bi-CG for solution of non-symmetric linear systems. *SIAM J. Sci. Stat. Comp.*, 13:631–644, 01 1992.